

## Supplementary Information

**Symmetry breaking structural phase transitions, dielectric properties and  
molecular motions of formamidinium cations  
in 1D and 2D hybrid compounds:  $(\text{NH}_2\text{CHNH}_2)_3[\text{Bi}_2\text{Cl}_9]$  and  
 $(\text{NH}_2\text{CHNH}_2)_3[\text{Bi}_2\text{Br}_9]$**

K. Mencil<sup>a</sup>, P. Starynowicz<sup>a</sup>, M. Siczek<sup>a</sup>, A. Piecha-Bisiorek<sup>a</sup>, R. Jakubas<sup>a</sup> and W. Medycki<sup>b</sup>

<sup>a</sup>*Faculty of Chemistry, University of Wrocław, Joliot-Curie 14, 50-383 Wrocław, Poland*

<sup>b</sup>*Institute of Molecular Physics, Polish Academy of Sciences, M. Smoluchowskiego 17, 60-179 Poznań, Poland*

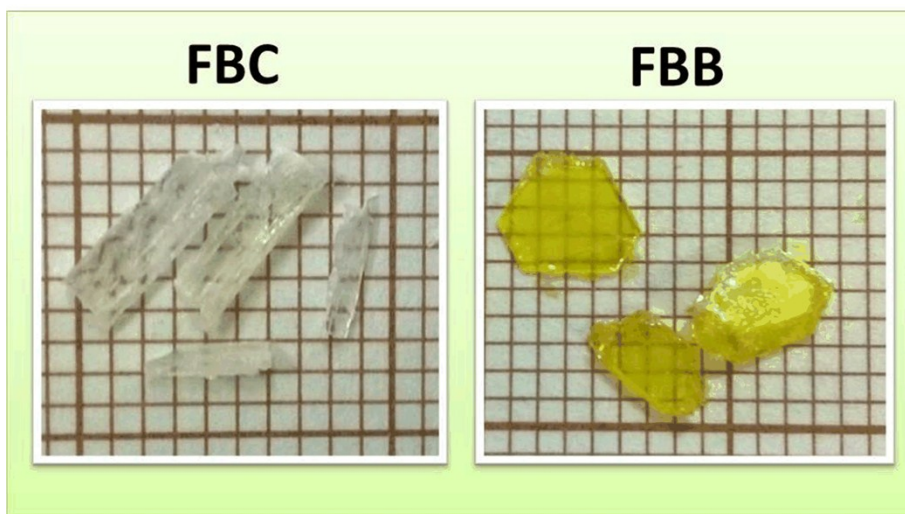


**Fig. S1.** The single crystals of **FBC** and **FBB**.

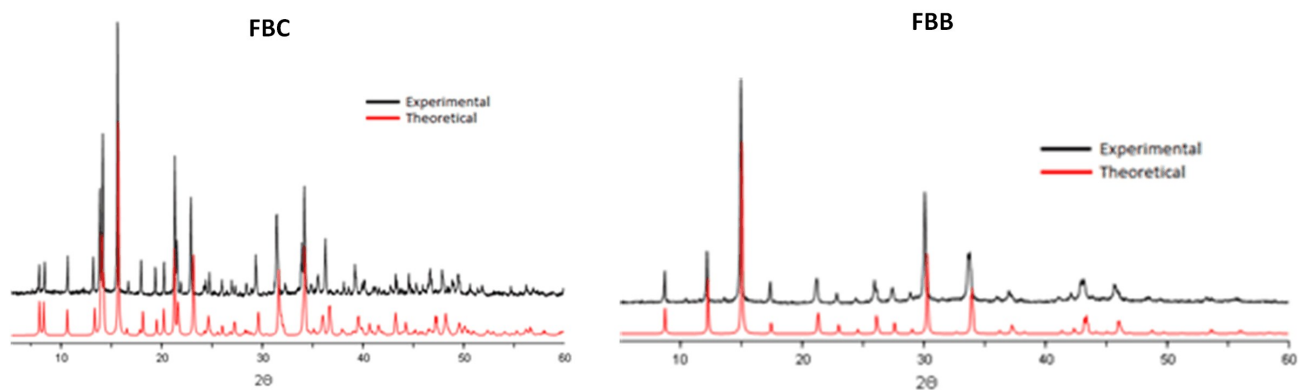


**Fig. S2.** Comparison between experimental powder XRD diffractogram of **FBC/FBB** and its simulated diffractogram.

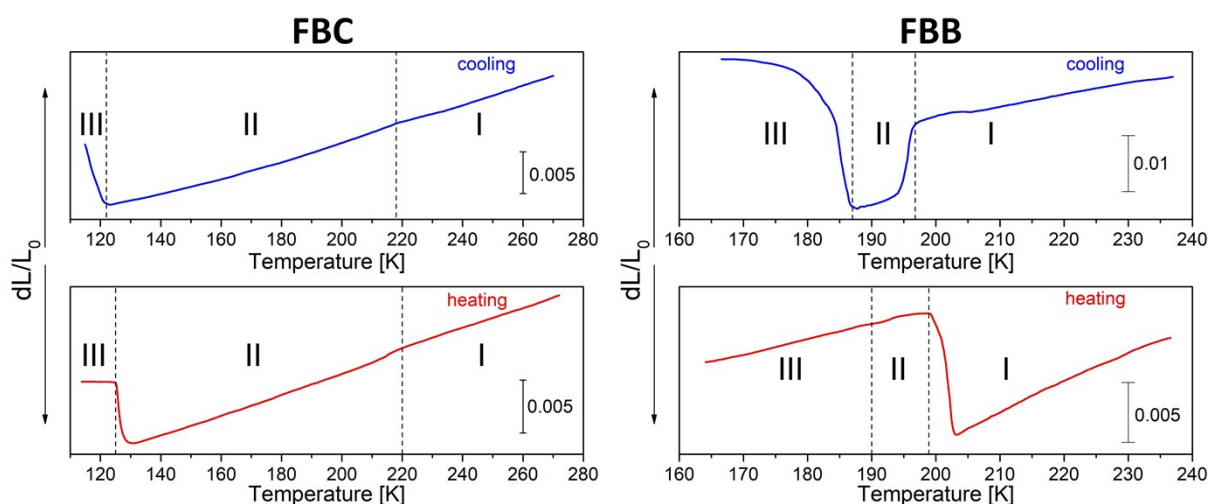


**Fig. S3.** Dilatometric measurements (the scanning rate of  $3 \text{ K}\cdot\text{min}^{-1}$ ) for **FBC** and **FBB**, respectively.

**Dilatometric measurements** for samples of **FBC** and **FBB** were carried out along the  $a$  and  $c$  directions, respectively. Results are presented in Fig. S3. For **FBC** crystal the sequence and nature of the phase transition obtained by the dilatometric measurements is consistent with the calorimetric studies. The high temperature PT is manifested only as a very subtle inflection of the baseline, what is typical for continuous PTs. Whereas the low temperature phase transition is characterized by a stepwise change in the crystal dimensions indicates the discontinuous character of this PT. In the case of a **FBB**, during cooling two anomalies of the linear thermal expansion,  $\Delta L/L_0$ , are visible. The transformation at 198 K and at 200 K, on cooling, are accompanied by a  $\Delta L/L_0$  change characteristic of a discontinuous transformation. During heating the PT (II→I) is associated with by a rapid increase of the dimensions of the sample. It should be noticed that the dilatometric anomaly around the PT (III→II) are not reversible on heating.

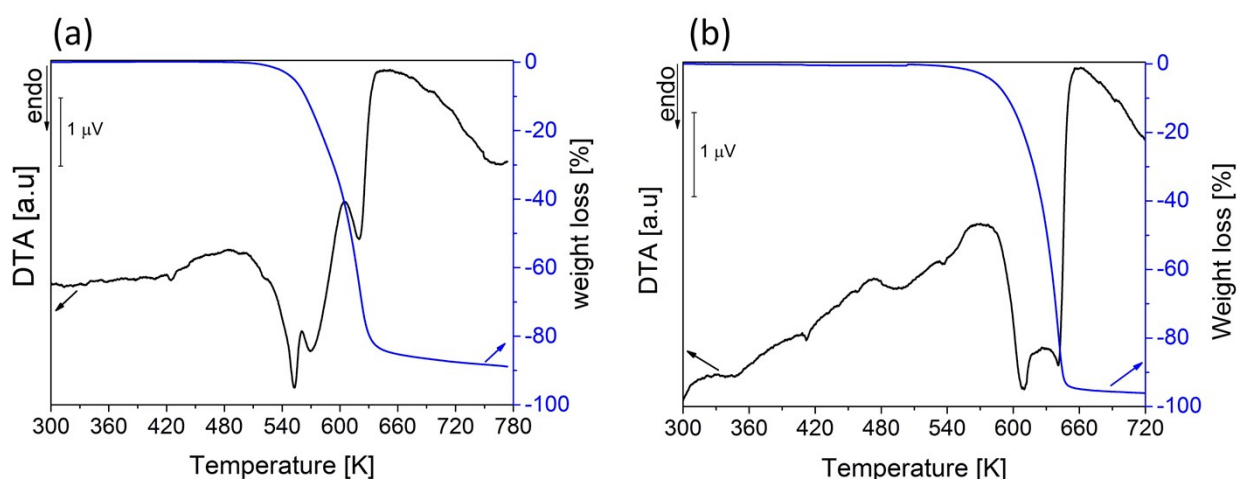


**Fig. S4.** Simultaneous thermogravimetric and differential thermal analyses scan (ramp rate:  $5 \text{ K}\cdot\text{min}^{-1}$ ) for (a) **FBC** and (b) **FBB**.

### *Nonabromodibismuthate(III) planes*

**Table S1.** Br-Bi-Br and Bi-Br-Bi angles (°) in I and III.

I			
<b>Br2<sup>i</sup>—Bi—Br2</b>	91.82 (11)	<b>Br2—Bi—Br1<sup>i</sup></b>	177.02 (8)
<b>Br2<sup>i</sup>—Bi—Br1</b>	90.25 (7)	<b>Bi—Br1—Bi<sup>iii</sup></b>	180.0
<b>Br1<sup>ii</sup>—Bi—Br1</b>	87.60 (6)		
III			
<b>Br3—Bi1—Br5</b>	92.06 (13)	<b>Br9—Bi2—Br10</b>	90.72 (15)
<b>Br3—Bi1—Br4</b>	91.89 (14)	<b>Br7—Bi2—Br11</b>	90.13 (13)
<b>Br5—Bi1—Br4</b>	91.53 (13)	<b>Br9—Bi2—Br11</b>	87.55 (15)
<b>Br3—Bi1—Br6</b>	88.56 (13)	<b>Br10—Bi2—Br11</b>	176.71 (13)
<b>Br5—Bi1—Br6</b>	88.01 (13)	<b>Br7—Bi2—Br11<sup>ii</sup></b>	176.91 (13)
<b>Br4—Bi1—Br6</b>	179.38 (14)	<b>Br9—Bi2—Br11<sup>ii</sup></b>	86.64 (14)
<b>Br3—Bi1—Br6<sup>i</sup></b>	87.46 (13)	<b>Br10—Bi2—Br11<sup>ii</sup></b>	84.80 (13)
<b>Br5—Bi1—Br6<sup>i</sup></b>	177.41 (13)	<b>Br11—Bi2—Br11<sup>ii</sup></b>	92.29 (5)
<b>Br4—Bi1—Br6<sup>i</sup></b>	85.95 (12)	<b>Br7—Bi2—Br8</b>	89.43 (13)
<b>Br6—Bi1—Br6<sup>i</sup></b>	94.51 (5)	<b>Br9—Bi2—Br8</b>	174.84 (14)
<b>Br3—Bi1—Br8</b>	174.52 (13)	<b>Br10—Bi2—Br8</b>	90.92 (13)
<b>Br5—Bi1—Br8</b>	91.87 (12)	<b>Br11—Bi2—Br8</b>	90.56 (13)
<b>Br4—Bi1—Br8</b>	91.82 (13)	<b>Br11<sup>ii</sup>—Bi2—Br8</b>	88.64 (13)
<b>Br6—Bi1—Br8</b>	87.77 (12)	<b>Bi1—Br6—Bi1<sup>iii</sup></b>	163.88 (18)
<b>Br6<sup>i</sup>—Bi1—Br8</b>	88.78 (12)	<b>Bi1—Br8—Bi2</b>	173.91 (15)
<b>Br7—Bi2—Br9</b>	95.37 (15)	<b>Bi2—Br11—Bi2<sup>iv</sup></b>	167.11 (17)
<b>Br7—Bi2—Br10</b>	92.82 (13)		

Symmetry codes for **I**: (i)  $-x+y+1, -x+1, z$ ; (ii)  $-y+1, x-y, z$ ; (iii)  $-x+1, -y, -z+1$ ; symmetry codes for **III**: (i)  $-x+1, y-1/2, -z+1/2$ ; (ii)  $-x, y+1/2, -z+1/2$ ; (iii)  $-x+1, y+1/2, -z+1/2$ ; (iv)  $-x, y-1/2, -z+1/2$ . N.B. Bi6, Bi8 and Bi11 belong to the Bi{1} family, the rest of Br atoms - to Br{2}.

### *Nonachlorodibismuthate(III) ribbons*

The Bi-Cl distances are listed in Table S2. In Phase I both Bi atoms, as well as Cl2, Cl3 and Cl5, are located on the mirror  $m \perp b$  plane, whereas in Phase II and III all Bi and Cl atoms are in general positions. The Bi-Cl distances vary among the phases generally within the limits of experimental error. Noteworthy are, however, short Bi1-Cl6, Bi21-Cl21 and Bi2-Cl4 bond lengths in Phase III in comparison with their parents (Bi2-Cl2 and Bi2-Cl4) in Phase I. Generally, bridging Cl{5} and Cl{6} atoms form longer Bi-Cl bonds than the terminal Cl atoms (the respective averages are 2.862 and 2.568 Å for Phase I, 2.869 and 2.566 Å for II, 2.859 and 2.562 Å for III).

**Table S2.** Bi-Cl distances (Å) in Phases I, II, III (FBC). Only symmetry independent bonds are listed.

I		II		III	
<b>Bi1—Cl1</b>	2.568 (4)	<b>Bi1—Cl1</b>	2.573 (6)	<b>Bi1—Cl1</b>	2.559 (6)
		<b>Bi1—Cl11</b>	2.568 (6)	<b>Bi1—Cl11</b>	2.563 (6)
		<b>Bi11—Cl12</b>	2.571 (7)	<b>Bi11—Cl12</b>	2.581 (6)
		<b>Bi11—Cl13</b>	2.570 (7)	<b>Bi11—Cl13</b>	2.575 (6)
<b>Bi1—Cl3</b>	2.566 (5)	<b>Bi1—Cl3</b>	2.569 (7)	<b>Bi1—Cl3</b>	2.567 (6)
		<b>Bi11—Cl31</b>	2.549 (8)	<b>Bi11—Cl31</b>	2.550 (6)

<b>Bi1—Cl5</b>	2.875 (4)	<b>Bi1—Cl5</b>	2.868 (8)	<b>Bi1—Cl5<sup>i</sup></b>	2.885 (7)
		<b>Bi11—Cl51<sup>ii</sup></b>	2.878 (9)	<b>Bi11—Cl51</b>	2.849 (7)
<b>Bi1—Cl6</b>	2.859 (4)	<b>Bi1—Cl6</b>	2.869 (7)	<b>Bi1—Cl6</b>	2.806 (6)
		<b>Bi1—Cl61</b>	2.847 (6)	<b>Bi1—Cl61<sup>iii</sup></b>	2.864 (6)
		<b>Bi11—Cl62</b>	2.844 (7)	<b>Bi11—Cl62</b>	2.834 (6)
		<b>Bi11—Cl63</b>	2.866 (7)	<b>Bi11—Cl63</b>	2.865 (6)
<b>Bi2—Cl2</b>	2.556 (4)	<b>Bi2—Cl2</b>	2.541 (8)	<b>Bi2—Cl2</b>	2.572 (7)
		<b>Bi21—Cl21</b>	2.564 (9)	<b>Bi21—Cl21</b>	2.512 (6)
<b>Bi2—Cl4</b>	2.571 (3)	<b>Bi2—Cl4</b>	2.568 (6)	<b>Bi2—Cl4</b>	2.540 (6)
		<b>Bi2—Cl41</b>	2.582 (7)	<b>Bi2—Cl41</b>	2.571 (6)
		<b>Bi21—Cl42</b>	2.573 (6)	<b>Bi21—Cl42</b>	2.579 (6)
		<b>Bi21—Cl43</b>	2.558 (6)	<b>Bi21—Cl43</b>	2.577 (6)
<b>Bi2—Cl5<sup>i</sup></b>	2.901 (4)	<b>Bi2—Cl5<sup>iv</sup></b>	2.898 (8)	<b>Bi2—Cl5</b>	2.902 (7)
		<b>Bi21—Cl51</b>	2.888 (9)	<b>Bi21—Cl51<sup>v</sup></b>	2.887 (7)
<b>Bi2—Cl6</b>	2.851 (4)	<b>Bi2—Cl6</b>	2.877 (6)	<b>Bi2—Cl6</b>	2.826 (6)
		<b>Bi2—Cl61<sup>iii</sup></b>	2.851 (7)	<b>Bi2—Cl61</b>	2.871 (6)
		<b>Bi21—Cl62</b>	2.881 (7)	<b>Bi21—Cl62<sup>vi</sup></b>	2.864 (6)
		<b>Bi21—Cl63<sup>iii</sup></b>	2.856 (6)	<b>Bi21—Cl63</b>	2.860 (6)

Symmetry codes: (i)  $-x+1, -y+1, -z+1$ ; (ii)  $-x+1, y+1/2, -z+1/2$ ; (iii)  $x, y-1, z$ ; (iv)  $-x+1/2, y-1/2, -z+1$ ; (v)  $-x, y+1/2, -z+1/2$ ; (vi)  $x, y+1, z$ .

More distinctly the Phase I→II and II→III PTs may be observed when geometry of the above mentioned rhombi is considered. In Phase I there is only one type of rhombi (for brevity hereinafter labelled as **rI**), namely that represented by Bi1-Bi2-Bi1<sup>i</sup>-Bi2<sup>i</sup> (see Fig. 2). Apart from the Bi-Cl distances its geometry may be described by the following angles: Bi1-Cl5-Bi2<sup>i</sup>, Cl5-Bi1-Cl6, Bi1-Cl6-Bi2 and Cl6-Bi2-Cl5<sup>i</sup>; the remaining angles are dependent as the rhombus is centrosymmetric. The relevant values (Table S3) show that the rhombus is essentially flat, as the Bi-Cl-Bi angles are very close to 180°. The Cl-Bi-Cl angles differ less than 3° from the right angle, what shows that the rhombus is a slightly distorted parallelepiped.

**Table S3.** Selected Cl-Bi-Cl and Bi-Cl-Bi angles (°)

I		II		III	
<b>Bi1—Cl5—Bi2<sup>i</sup></b>	179.78 (19)	<b>Bi1—Cl5—Bi2<sup>ix</sup></b>	177.0 (3)	<b>Bi1<sup>i</sup>—Cl5—Bi2</b>	178.5 (3)
		<b>Bi11<sup>x</sup>—Cl51—Bi21</b>	178.6 (3)	<b>Bi11—Cl51—Bi21<sup>xi</sup></b>	175.3 (3)
<b>Cl6—Bi1—Cl5</b>	87.34 (12)	<b>Cl5—Bi1—Cl6</b>	85.8 (2)	<b>Cl6—Bi1—Cl5<sup>i</sup></b>	87.33 (19)
		<b>Cl61—Bi1—Cl5</b>	86.5 (2)	<b>Cl61<sup>iii</sup>—Bi1—Cl5<sup>i</sup></b>	88.66 (18)
		<b>Cl62—Bi11—Cl51<sup>ii</sup></b>	87.5 (2)	<b>Cl51—Bi11—Cl63</b>	84.88 (18)
		<b>Cl63—Bi11—Cl51<sup>ii</sup></b>	86.2 (2)	<b>Cl62—Bi11—Cl51</b>	86.93 (18)
<b>Bi2—Cl6—Bi1</b>	178.99 (16)	<b>Bi1—Cl6—Bi2</b>	171.7 (3)	<b>Bi1—Cl6—Bi2</b>	170.5 (3)
		<b>Bi1—Cl61—Bi2<sup>vi</sup></b>	170.6 (3)	<b>Bi1<sup>vi</sup>—Cl61—Bi2</b>	170.6 (2)
		<b>Bi11—Cl62—Bi21</b>	171.0 (3)	<b>Bi21—Cl63—Bi11</b>	165.7 (2)
		<b>Bi21<sup>vi</sup>—Cl63—Bi11</b>	172.9 (3)	<b>Bi11—Cl62—Bi21<sup>iii</sup></b>	164.8 (2)
<b>Cl6—Bi2—Cl5<sup>i</sup></b>	93.82 (11)	<b>Cl6—Bi2—Cl5<sup>iv</sup></b>	93.4 (2)	<b>Cl6—Bi2—Cl5</b>	90.89 (19)
		<b>Cl61<sup>iii</sup>—Bi2—Cl5<sup>iv</sup></b>	97.2 (2)	<b>Cl61—Bi2—Cl5</b>	95.97 (18)
		<b>Cl62—Bi21—Cl51</b>	96.1 (2)	<b>Cl63—Bi21—Cl51<sup>v</sup></b>	93.41 (18)

		<b>Cl6<sup>3iii</sup>—Bi21—Cl51</b>	93.0 (2)	<b>Cl6<sup>2vi</sup>—Bi21—Cl51<sup>v</sup></b>	99.65 (18)
<b>Cl6—Bi1—Cl6<sup>vii</sup></b>	84.28 (18)	<b>Cl61—Bi1—Cl6</b>	84.9 (3)	<b>Cl6—Bi1—Cl61<sup>iii</sup></b>	83.3 (2)
		<b>Cl62—Bi11—Cl63</b>	85.0 (2)	<b>Cl62—Bi11—Cl63</b>	84.10 (18)
<b>Cl6—Bi2—Cl6<sup>viii</sup></b>	84.45 (18)	<b>Cl61<sup>iii</sup>—Bi2—Cl6</b>	83.8 (3)	<b>Cl6—Bi2—Cl61</b>	83.7 (2)
		<b>Cl6<sup>3iii</sup>—Bi21—Cl62</b>	83.6 (2)	<b>Cl63—Bi21—Cl6<sup>2vi</sup></b>	83.12 (18)

The symmetry codes are those from Table S2, apart from that: (vii)  $x, -y+1/2, z$ ; (viii)  $x, -y+3/2, z$ , (ix)  $-x+1/2, y+1/2, -z+1$ ; (x)  $-x+1, y-1/2, -z+1/2$ ; (xi)  $-x, y-1/2, -z+1/2$ ;

In **II** there are two independent ribbons. The first one is formed by Bi, Bi2, Cl5, C6, Cl61, as well as by terminal Cl1, Cl11, Cl2, Cl3, Cl4 and Cl41 atoms. Here is only one type of rhombi (**rIIICl5**): Bi1-(Cl6)-Bi2-(Cl5<sup>iv</sup>)-Bi1<sup>iv</sup>-(Cl61<sup>iv</sup>)-Bi2<sup>ix</sup>-(Cl5). The other ribbon is formed by rhombi spanned by Bi11-(Cl62)-Bi21-(Cl51)-Bi11<sup>x</sup>-(Cl63<sup>x</sup>)-Bi21<sup>ii</sup>-(Cl51<sup>ii</sup>) (**rIIICl51**). In **III** there are also two different ribbons. The first one is composed of two types of alternating centrosymmetric rhombi: Bi1-(Cl6)-Bi2-(Cl5)-Bi1<sup>i</sup>-(Cl6<sup>i</sup>)-Bi2<sup>1</sup>-(Cl5<sup>i</sup>) (**rIIICl5/Cl6**) and Bi1-(Cl5<sup>1</sup>)-Bi2<sup>i</sup>-(Cl61<sup>i</sup>)-Bi1<sup>xxiii</sup>-(Cl5<sup>iii</sup>)-Bi2<sup>iii</sup>-(Cl61<sup>iii</sup>) (**rIIICl5/Cl61**). Please note that the symmetry operations have been selected so to close the figures (loops); in Table S3 equivalent angles are listed. The other ribbon is composed of rhombi of one type: Bi11-(Cl63)-Bi21-(Cl51<sup>v</sup>)-Bi11<sup>v</sup>-(Cl62<sup>v</sup>)-Bi21<sup>v</sup>-(Cl51) (**rIIICl51**). A view of all the rhombi along the Bi{1}-Cl{5}-Bi{2} direction shows the essential differences between the phases (Fig. S5). In Phase **I** the constituent rhombus is practically flat, whereas in **II** both **rIIICl5** and **rIIICl51** are bent along the Cl{6}-Cl{6}' axis, the bending is approximately 7-10°; see Table S3 for the exact values of the Bi{1}-Cl{6}-Bi{2} angles. In Phase **III** two rhombi, forming the ribbon with Bi1 and Bi2, **rIIICl5/Cl6** and **rIIICl5/Cl61** are warped; this is a consequence of their centrosymmetry (see Fig. 4). The third rhombus, **rIIICl51**, is bent in a way similar to those in **II**, but the bending (*ca.* 15°) is greater. On the other hand the Bi{1}-(Cl{5})-Bi{2} sides remain rather undistorted, as the Bi{1}-Cl{5}-Bi{2} angles do not deviate much from 180°, the largest deviation being 4.7 (3)° for Bi11—Cl51—Bi21<sup>xi</sup>. In **II** the ribbons of different types are shifted with respect to each other *ca.* 0.24 Å along the **b** direction; in **III** – 0.29 Å. In all three phase inclination of the adjacent rhombi, as measured by the Cl{6}-Bi{1}-Cl{6}' and Cl{6}-Bi{2}-Cl{6}' angles remains practically unchanged, being in the range 83-85°.

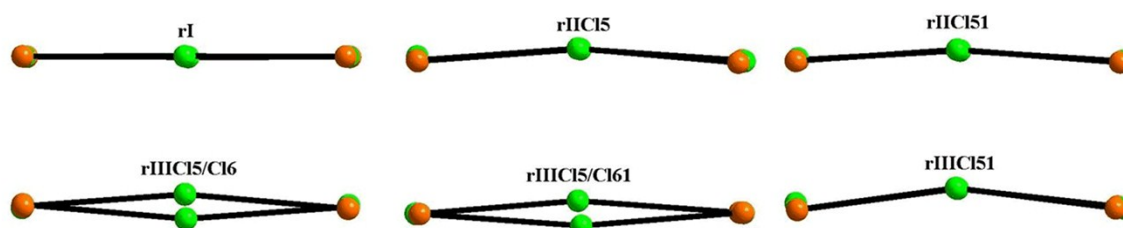


**Fig. S5.** A view of the constituent rhombi along the Bi{1}-Cl{5}-Bi{2} direction; see the text for the explanations.

### Hydrogen bonds in FBC

The hydrogen bonds in the presented structures are listed in Table S4; for the reader's convenience the parent C atoms in the formamidinium cations are listed in the first column. The bonds are exclusively of the N-H...Cl type and generally are rather weak. If, as it is commonly accepted, formation of the hydrogen bond is recognized when the D...A distance is smaller than the sum of Van der Waals radii of the donor and acceptor, only such N...Cl pairs may be safely regarded as connected via an H-bond, if the N...Cl distance is shorter than 3.3-3.4 Å [1, 2]. In Phase I and III weak bifurcated H-bonds have been found. In Phase I H4A, H5B and H51B are involved in such interactions, moreover, H41B is the centre of a trifurcate bond. In Phase III bifurcate bonds/interactions are mediated by H2B, H4A, H7A and H12A. The general weakness of the hydrogen bonds in the described structures may be one of the factors that facilitate the phase transitions.

**Table S4.** N-H...Cl hydrogen bonds and contacts in FBC.

parent C atom		D-H (Å)	H...A (Å)	D...A (Å)	∠DHA (°)
	I				
C1	N1-H1A...Cl2 <sup>xii</sup>	0.86	2.73	3.35(3)	130
C1	N1-H1B...Cl4 <sup>xiii</sup>	0.86	2.50	3.31(2)	157
C1	N2-H2A...Cl1 <sup>xiv</sup>	0.92	2.82	3.00(3)	92
C1	N2-H2A...Cl1 <sup>xv</sup>	0.92	2.75	3.64(3)	164
C1	N2-H2B...Cl1 <sup>xiv</sup>	0.86	2.64	3.00(3)	107
C2	N3-H3B...Cl5 <sup>vi</sup>	0.86	2.53	3.23(4)	138
C21	N31-H31B...Cl5 <sup>vi</sup>	0.87	2.85	3.71(5)	170
C2	N4-H4A...Cl4 <sup>xvii</sup>	0.86	2.74	3.38(4)	133
C2	N4-H4A...Cl4 <sup>xviii</sup>	0.86	2.74	3.38(4)	133
C2	N4-H4B...Cl3 <sup>i</sup>	0.86	2.57	3.34(4)	150
C21	N41-H41B...Cl1 <sup>xiv</sup>	0.86	2.69	3.29(4)	128
C21	N41-H41B...Cl1 <sup>xv</sup>	0.86	2.69	3.29(4)	128
C21	N41-H41B...Cl3 <sup>i</sup>	0.86	2.82	3.18(5)	107
C3	N5-H5B...Cl4 <sup>xix</sup>	0.86	2.59	3.21(4)	129
C3	N5-H5B...Cl4 <sup>xx</sup>	0.86	2.59	3.21(4)	129
C31	N51-H51A...Cl5 <sup>xxi</sup>	0.86	2.46	3.20(6)	144
C31	N51-H51B...Cl4 <sup>xix</sup>	0.86	2.78	3.37(4)	127
C31	N51-H51B...Cl4 <sup>xx</sup>	0.86	2.78	3.37(4)	127
C31	N61-H61B...Cl2	0.85	2.88	3.36(5)	118
	II				
C1	N1-H1A...Cl43 <sup>xxii</sup>	0.86	2.80	3.34(2)	123
C1	N1-H1B...Cl42 <sup>xxiii</sup>	0.86	2.58	3.40(2)	159
C1	N2-H2A...Cl21 <sup>xxii</sup>	0.86	2.78	3.52(2)	144
C1	N2-H2B...Cl11 <sup>v</sup>	0.86	2.66	3.29(2)	131
C11	N3-H3A...Cl2 <sup>xxiv</sup>	0.86	2.84	3.32(3)	120
C11	N3-H3B...Cl4 <sup>vi</sup>	0.86	2.45	3.31(2)	177
C11	N4-H4A...Cl41 <sup>xxiv</sup>	0.86	2.68	3.43(3)	146
C11	N4-H4B...Cl13 <sup>iv</sup>	0.86	2.75	3.30(3)	123
C2	N5-H5A...Cl42 <sup>xxv</sup>	0.86	2.64	3.429(2)	171
C2	N5-H5B...Cl3 <sup>xxvi</sup>	0.86	2.68	3.30(2)	131
C2	N6-H6A...Cl63 <sup>xxvii</sup>	0.86	2.79	3.34(3)	123
C2	N6-H6B...Cl5 <sup>xxiii</sup>	0.86	2.67	3.48(3)	157
C21	N7-H7A...Cl41 <sup>iv</sup>	0.86	2.68	3.52(3)	165
C21	N7-H7B...Cl31 <sup>xxvii</sup>	0.86	2.61	3.33(3)	143

C22	N7-H7C...CI11	0.86	2.67	3.49(3)	160
C22	N7-H7D...CI31 <sup>xxvii</sup>	0.86	2.74	3.33(3)	128
C21	N8-H8A...CI6 <sup>iv</sup>	0.86	2.88	3.66(3)	153
C21	N8-H8B...CI5 <sup>iv</sup>	0.86	2.80	3.41(3)	129
C22	N8-H8C...CI6	0.86	2.83	3.64(3)	156
C22	N8-H8D...CI5 <sup>iv</sup>	0.86	2.75	3.41(3)	135
C3	N9-H9A...CI61 <sup>iii</sup>	0.86	2.81	3.45(3)	132
C3	N10-H10A...CI1 <sup>iii</sup>	0.86	2.61	3.41(4)	153
C3	N10-H10B...CI42 <sup>xxviii</sup>	0.86	2.59	3.31(4)	143
C31	N11-H11B...CI21 <sup>xxvii</sup>	0.86	2.83	3.35(3)	121
C32	N11-H11C...CI1	0.86	2.76	3.56(3)	155
C32	N11-H11D...CI21 <sup>xxvii</sup>	0.86	2.74	3.35(3)	130
C31	N12-H12B...CI4 <sup>ix</sup>	0.86	2.85	3.41(3)	124
C32	N12-H12C...CI5	0.86	2.83	3.65(3)	159
C32	N12-H12D...CI4 <sup>ix</sup>	0.86	2.83	3.41(3)	127
	III				
C1	N1-H1A...CI21	0.86	2.73	3.30(2)	125
C1	N1-H1B...CI42 <sup>xxix</sup>	0.86	2.42	3.27(2)	172
C1	N2-H2A...CI43	0.86	2.67	3.47(2)	155
C1	N2-H2B...CI1 <sup>xxx</sup>	0.86	2.72	3.24(2)	121
C1	N2-H2B...CI11 <sup>xxxi</sup>	0.86	2.83	3.52(2)	138
C11	N3-H3B...CI41	0.86	2.49	3.34(2)	168
C11	N4-H4A...CI2 <sup>iii</sup>	0.86	2.87	3.48(2)	130
C11	N4-H4A...CI41 <sup>x</sup>	0.86	2.75	3.43(2)	137
C11	N4-H4B...CI13 <sup>x</sup>	0.86	2.63	3.24(2)	129
C2	N5-H5A...CI63 <sup>x</sup>	0.86	2.70	3.50(3)	155
C2	N5-H5B...CI51 <sup>xxxii</sup>	0.86	2.71	3.40(3)	138
C2	N6-H6A...CI13 <sup>x</sup>	0.86	2.47	3.32(2)	168
C2	N6-H6B...CI3	0.86	2.71	3.31(3)	128
C21	N7-H7A...CI1 <sup>i</sup>	0.86	2.86	3.42(2)	125
C21	N7-H7A...CI11 <sup>xxxiii</sup>	0.86	2.71	3.44(2)	143
C21	N7-H7B...CI31	0.86	2.69	3.27(3)	126
C21	N8-H8A...CI61 <sup>i</sup>	0.86	2.83	3.56(4)	144
C21	N8-H8A...CI5 <sup>i</sup>	0.86	2.64	3.33(4)	138
C3	N9-H9A...CI61	0.86	2.61	3.44(2)	162
C3	N9-H9B...CI2	0.86	2.80	3.38(2)	126
C3	N10-H10A...CI11 <sup>vi</sup>	0.86	2.58	3.40(2)	159
C3	N10-H10A...CI42 <sup>xxxii</sup>	0.86	2.53	3.30(2)	150
C31	N11-H11A...CI5	0.86	2.75	3.54(3)	153
C31	N11-H11B...CI4	0.86	2.78	3.38(3)	129
C31	N12-H12A...CI1 <sup>i</sup>	0.86	2.58	3.44(3)	173
C31	N12-H12A...CI21	0.86	2.68	3.41(3)	143

The symmetry codes are those from Tables S2 and S3, apart from that: (xii)  $x, y, z+1$ ; (xiii)  $-x+1, y-1/2, -z+1$ ; (xiv)  $x+1/2, y+1, -z+3/2$ ; (xv)  $x+1/2, -y+1/2, -z+3/2$ ; (xvi)  $-x+3/2, -y+1, z+1/2$ ; (xvii)  $-x+3/2, y-1/2, z+1/2$ ; (xviii)  $-x+3/2, -y+2, z+1/2$ ; (xix)  $x-1/2, y, -z+1/2$ ; (xx)  $x-1/2, -y+3/2, -z+1/2$ ; (xxi)  $-x+1/2, -y+1, z-1/2$ ; (xxii)  $x-1/2, -y+3/2, z$ ; (xxiii)  $x-1/2, -y+1/2, z$ ; (xxiv)  $-x+1/2, -y+1, -z+3/2$ ; (xxv)  $-x+1/2, -y, -z+1/2$ ; (xxvi)  $-x, -y+1, -z+1$ ; (xxvii)  $-x+1/2, -y+1, -z+1/2$ ; (xxviii)  $x-1/2, y, z+1/2$ ; (xxix)  $-x, 2-y, 1-z$ ; (xxx)  $x-1, y, z$ ; (xxxi)  $x-1, y+1, z$ ; (xxxii)  $x+1, y, z$ ; (xxxiii)  $-x+1, -y, -z+1$ ;

### **Hydrogen bonds in FBB**

As previously, it may be noticed that the N-H $\cdots$ Br interactions, collected in Table S5, are rather weak. Only those contacts may be regarded as hydrogen bonds, for which the N $\cdots$ Br distance is smaller than 3.4-3.5 Å.<sup>1-2</sup> In Phase I a weak symmetric bifurcated H-bond (that mediated by H111) is present. In Phase III this symmetry breaks down and only trace of the bifurcation may be observed (in the bond mediated by H5B).

**Table S5.** N-H $\cdots$ Br hydrogen bonds and contacts in FBB.

parent C atom	D—H $\cdots$ A	D—H (Å)	H $\cdots$ A (Å)	D $\cdots$ A (Å)	D—H $\cdots$ A (°)
<b>I</b>					
C11	N11—H111 $\cdots$ Br2 <sup>i</sup>	0.94	2.84	3.30(2)	112
C11	N11—H111 $\cdots$ Br2 <sup>ii</sup>	0.94	2.84	3.30(2)	112
C11	N11—H112 $\cdots$ Br1	0.88	2.80	3.60(5)	151
C11	N21—H211 $\cdots$ Br2 <sup>iii</sup>	0.87	2.49	3.28(5)	151
C11	N21—H212 $\cdots$ Br2 <sup>iv</sup>	0.87	2.36	3.17(5)	156
C12	N12—H12B $\cdots$ Br2 <sup>ii</sup>	0.94	2.87	3.25(5)	105
C12	N22—H22A $\cdots$ Br1 <sup>v</sup>	0.87	2.23	3.02(7)	152
C12	N22—H22B $\cdots$ Br2 <sup>vi</sup>	0.87	2.39	3.12(5)	142
<b>III</b>					
C3	N1—H1A $\cdots$ Br5 <sup>i</sup>	0.88	2.79	3.64(3)	162.4
C3	N1—H1B $\cdots$ Br8	0.88	2.74	3.52(3)	149.2
C4	N2—H2A $\cdots$ Br4 <sup>ii</sup>	0.88	2.86	3.68(4)	156.6
C4	N2—H2B $\cdots$ Br3 <sup>iii</sup>	0.88	2.60	3.45(4)	161.8
C4	N3—H3A $\cdots$ Br3 <sup>ii</sup>	0.88	2.80	3.54(4)	143.0
C4	N3—H3B $\cdots$ Br10	0.88	2.57	3.39(4)	154.4
C3	N4—H4A $\cdots$ Br8 <sup>i</sup>	0.88	2.93	3.49(4)	123.4
C3	N4—H4B $\cdots$ Br10 <sup>i</sup>	0.88	2.66	3.54(4)	173.5
C19	N5—H5A $\cdots$ Br10 <sup>iv</sup>	0.88	2.78	3.59(6)	152.5
C19	N5—H5B $\cdots$ Br9 <sup>v</sup>	0.88	2.92	3.38(5)	114.7
C19	N5—H5B $\cdots$ Br11 <sup>v</sup>	0.88	2.87	3.72(7)	161.4
C19	N6—H6A $\cdots$ Br10 <sup>iv</sup>	0.88	2.91	3.66(5)	145.0
C19	N6—H6B $\cdots$ Br9 <sup>vi</sup>	0.88	2.47	3.33(4)	167.4

Symmetry codes for I: (i)  $-y, x-1, z$ ; (ii)  $-x+y+1, -x+1, z$ ; (iii)  $-x+1, -x+y, -z$ ; (iv)  $-x+y+1, -x, z$ ; (v)  $x-1, y, z$ ; (vi)  $x-y-1, -y, -z+1$ ; symmetry codes for II: (i)  $x, y-1, z$ ; (ii)  $-x+1, y+1/2, -z+1/2$ ; (iii)  $-x+1, y-1/2, -z+1/2$ ; (iv)  $x, -y+1/2, z-1/2$ ; (v)  $-x, y+1/2, -z+1/2$ ; (vi)  $-x, y-1/2, -z+1/2$ .

**Dielectric dispersion results**

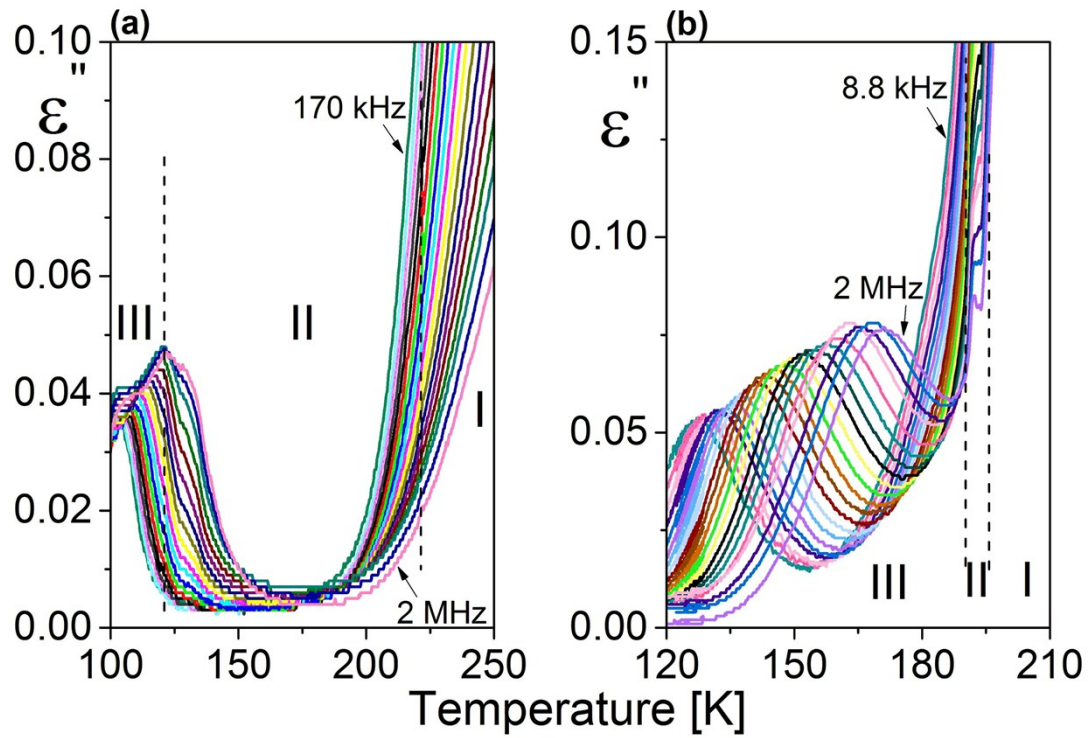


**Fig. S6.** The temperature dependence of the imaginary part of the complex electric permittivity of the (a) FBC and (b) FBB crystal.

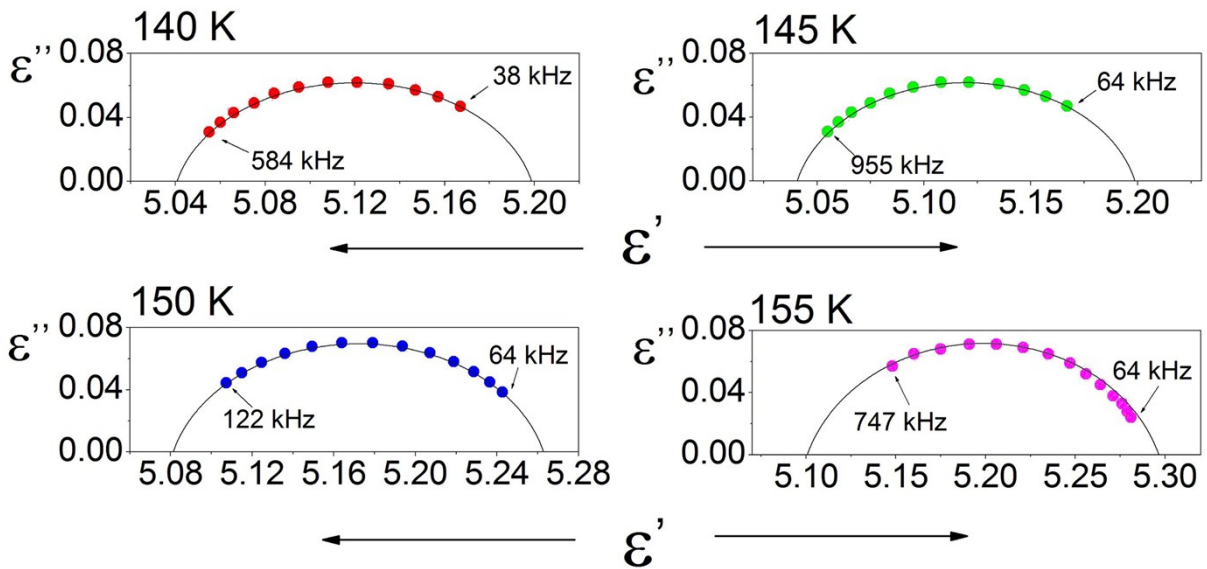


**Fig. S7.** Cole–Cole plots of  $\epsilon''$  versus  $\epsilon'$  at selected temperatures showing the relaxation nature of the dielectric dispersion for FBB.

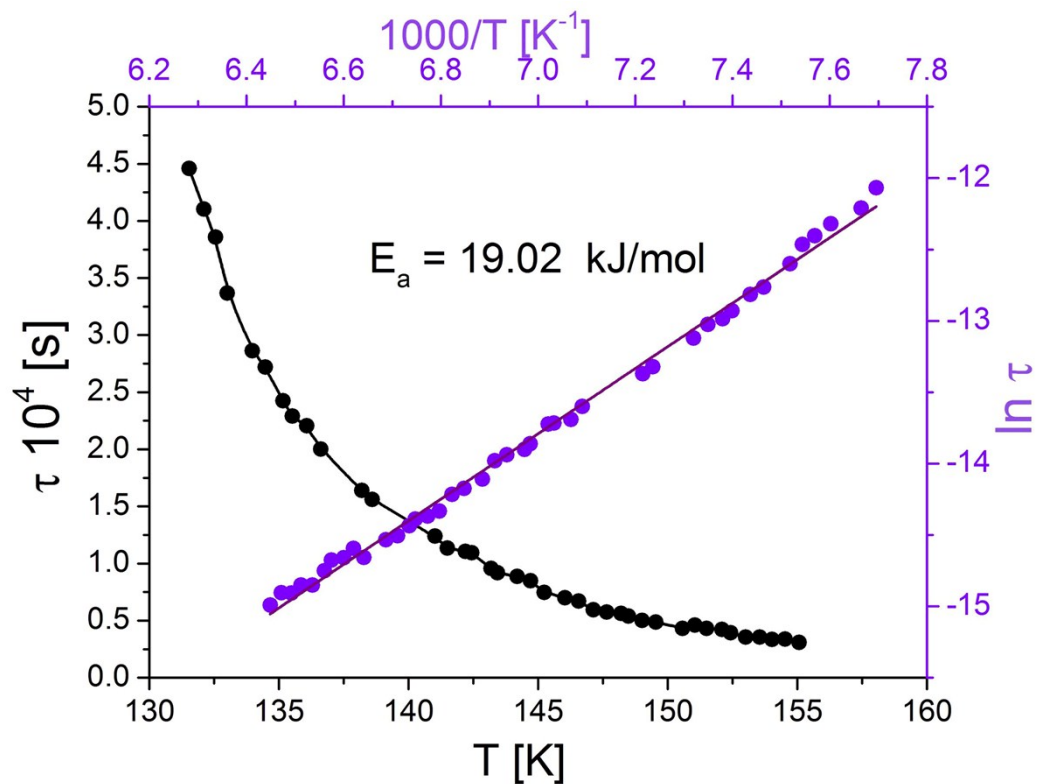


Fig. S8. Temperature dependence of the macroscopic relaxation time (s) and its inverse (s<sup>-1</sup>) in FBB.

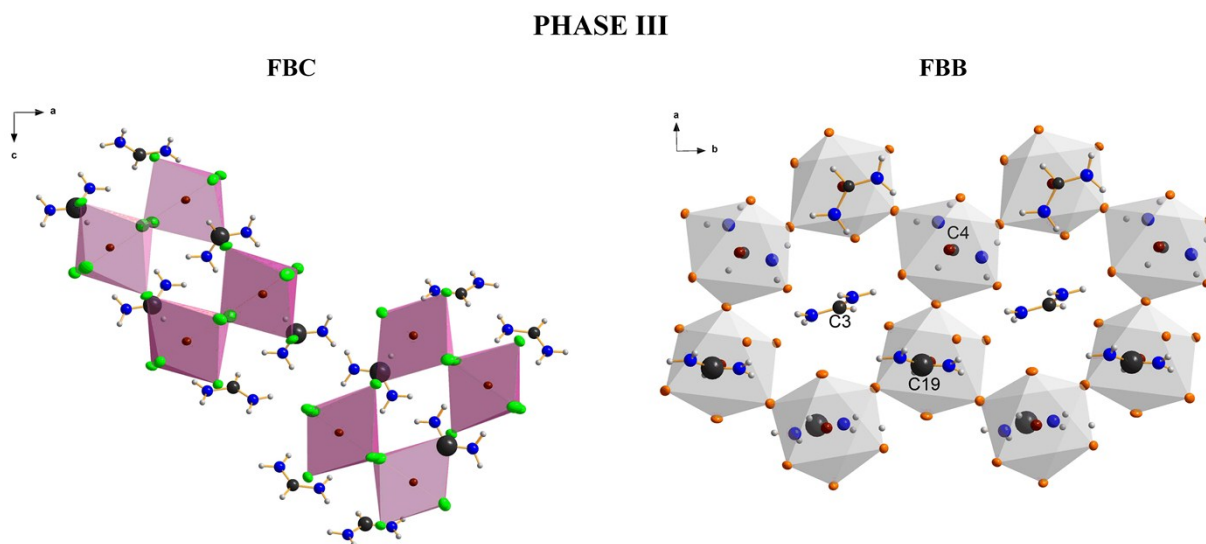


Fig. S9. The crystal structure of (a) FBC (the view along the  $b$ -axis) and (b) FBB (the view along the  $c$ -axis) in phase III with FA<sup>+</sup> cations.

### Ferroelastic domain structure of FBB

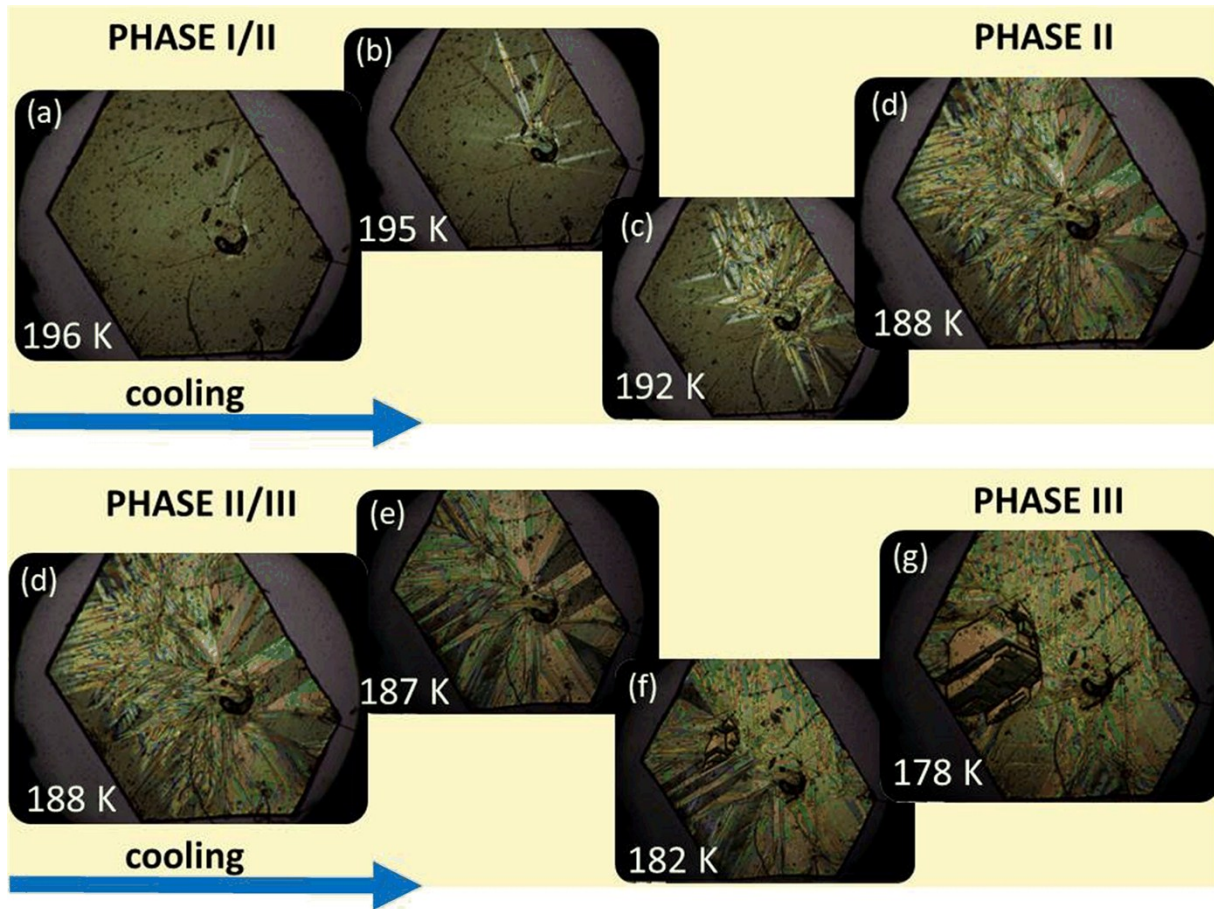


Fig. S10. The evolution of the ferroelastic domain pattern for **FBB** during the cooling cycle.

Fig. S10 shows the appearance of the ferroelastic domain structure through the PT(I→II) (Fig. S10 a-b) and strong twinning through (II→III) (Fig. S10 d-e).

### Second moment of $^1\text{H}$ NMR for FBC

The theoretical calculation of the dipolar second moment  $M_2$  for the rigid structure obtained from XRD was derived by van Vleck<sup>3</sup>:

$$M_2 = \frac{3}{5} I(I+1) \gamma^2 \hbar^2 \frac{1}{N} \sum_{i=1}^N \sum_{j=1}^N R_{ij}^{-6} \quad (1)$$

where  $N$  is the number of protons in the unit cell,  $R_{ij}$  are distances between interacting protons. The rigid value of  $M_2$  calculated from the crystal structure appeared to be about 12.2 G<sup>2</sup> with assumed lengths of bonds: C-H 1.09 Å and N-H 1.03 Å (please note, that the positions of hydrogen nuclei are only theoretically estimated). The obtained result is twice lower than that found from the experimental plateau for formamidinium iodide 24 G<sup>2</sup>.<sup>4</sup> The reason of it is that assumed length of N-H bond (1.03 Å), usually used in NMR data analysis is

in fact, shorter and equals 0.9 Å. On the other hand, the effect of quadrupole interaction of the chlorine atoms is not excluded.

The second-moment of  $^1\text{H}$  NMR line for **FBC** (Fig. S11) shows that between 100 and 290 K the value of the  $M_2$  is continuously reduced from about 10  $\text{G}^2$  to about 3  $\text{G}^2$ .

The first reduction is caused probably by start-up of axial rotation of whole formamidinium cation around the axis parallel to N – N line after breaking the hydrogen bonds. Please note, that for **FBC** the reached  $M_2$  value above 160 K is practically equals to  $\frac{1}{4}$  of the second moment value before reduction (expected 6  $\text{G}^2$ ) and this fact denotes that all formamidinium cations perform freely axial rotations. In turn, the next reduction is the onset of motion of parts of formamidinium cations in the disorder state.

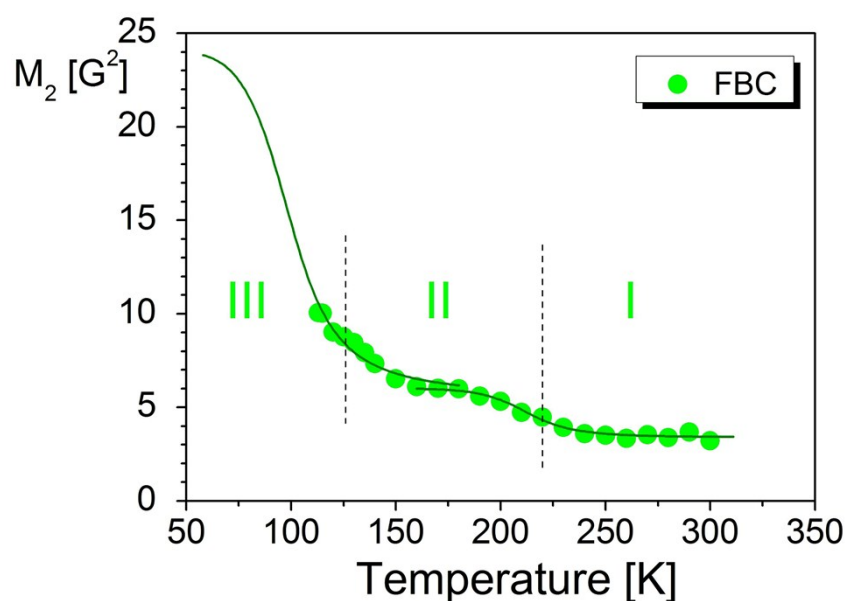


**Fig. S11.** Temperature dependence of  $M_2$  for **FBC** (green points) and theoretical calculations (solid line), the results of fitting :  $E_{a1} = 1.08 \text{ kcal mol}^{-1}$ ,  $\tau_{01} = 4.22 \cdot 10^{-8} \text{ s}$ ,  $E_{a2} = 5.77 \text{ kcal} \cdot \text{mol}^{-1}$ ,  $\tau_{02} = 2.08 \cdot 10^{-11} \text{ s}$ .

**Table S6.** The obtained fitting parameters for **FBB** (eq. 1).

Parameter	FBB
$E_{a1} [\text{kcal mol}^{-1}]$	2.68
$\tau_{01} [\text{s}]$	$2.36 \cdot 10^{-13}$
$C_1 [\text{s}^{-2}]$	$1.3 \cdot 10^9$
$E_{a2} [\text{kcal mol}^{-1}]$	4.97
$\tau_{02} [\text{s}]$	$5.36 \cdot 10^{-15}$
$C_2 [\text{s}^{-2}]$	$6.5 \cdot 10^8$

- 1 A. Bondi, J. Phys. Chem., 1964, **68**, 441.
- 2 S. S. Batsanov, Inorg. Materials, 2001, **37**, 871.
- 3 J. H. Van Vleck, Phys. Rev., 1948, **74**, 1168.
- 4 K. Mencil, P. Durlak, M. Rok, R. Jakubas, J. Baran, W. Medycki, A. Cizman and A. Piecha-Bisiorek, RSC Adv., 2018, **8**, 26506.